Excitonic effects on the third-harmonic generation in parabolic quantum dots

2001 J. Phys.: Condens. Matter 13 8197

(http://iopscience.iop.org/0953-8984/13/35/324)

INSTITUTE OF PHYSICS PUBLISHING JOURNAL OF PHYSICS: CONDENSED MATTER

J. Phys.: Condens. Matter **13** (2001) 8197–8206 PII: S0953-8984(01)25145-5

Excitonic effects on the third-harmonic generation in parabolic quantum dots

Guanghui Wang[1] **and Kangxian Guo**

Department of Physics, Guihuagang Campus, Guangzhou University, Guangzhou 510405, People's Republic of China

E-mail: gsnuwgh@263.net (Guanghui Wang)

Received 24 May 2001, in final form 12 July 2001
Published 16 August 2001
Online at stacks.iop.org/JPhysCM/13/8197

Abstract

Excitonic effects on the third-harmonic-generation coefficient for disclike parabolic quantum dots are studied, and an analytic formula for the third-harmonic-generation coefficient is obtained by using the compact-density-matrix approach and an iterative method. Numerical results are presented for typical GaAs/AlGaAs parabolic quantum dots. The results show that the third-harmonic-generation coefficient is greatly enhanced because the excitons are localized in the quantum dots—it is over three times that obtained by just considering electron states—and that it is very sensitively dependent on the exciton confinement. In addition, the third-harmonic-generation coefficient is related to the relaxation constant.

1. Introduction

Recently the excitonic states in semiconductor quantum wells, superlattices, and nanostructures have attracted much attention from the fundamental physics viewpoint and also as regards applied physics, owing to the enhanced excitonic optical nonlinearity and fast response time [1, 2]. Excitons in quantum dots have been observed in photoluminescence experiments performed on multidot samples [3] and single-dot samples [4].

In 1975, Esaki *et al* were the first to present the concept of quantum wires and dots [5]. With recent rapid advances of modern technology, it has now become possible to produce quasi-zero-dimensional systems that confine electrons in all three spatial dimensions by using techniques such as etching or using metal grid gates [6]. They typically have a disclike shape, a few hundred nanometres in diameter and a few nanometres thick. In such nanometre structures, electrons are not only confined in all three spatial dimensions, but also are quantized into discrete energy levels, with energy spacings of a few meV or more [7]. Recently, the quantum dots with (quasi-) 0D structures have become more and more important because of

[1] Author to whom any correspondence should be addressed.

their novel physical properties and promise for potential applications. Sauvage and Boucaud discussed nonlinear optical properties of quantum dots [8], but they did not consider excitonic effects. However, in semiconductor quantum dots, carriers are confined in three spatial dimensions, which substantially enhances the overlap between holes and electron clouds, and leads to enhancement of the Coulomb binding energy and oscillator strength, so it is clearly very important to consider excitonic effects. In 1988, Eiichi Hanamura studied theoretically the nonlinear optical properties of semiconductor microcrystallites, and showed that optical nonlinearities are very large when one considers exciton effects [9]. In 1993, Chen *et al* discussed the third-order nonlinear optical susceptibility in Si quantum wires, and also obtained enhancement of the nonlinear optical properties due to excitonic effects [10].

In this paper, excitonic effects on the third-harmonic generation in disclike parabolic quantum dots are studied. These have rarely been discussed in the literature. In section 2 the eigenfunctions and eigenenergies of the exciton states are obtained using the effective-mass approximation, with centre-of-mass and relative coordinates. In section 3 an analytical formula for the third-harmonic-generation coefficient is derived by using the compact-density-matrix approach and an iterative method. In section 4 we calculate the third-harmonic-generation coefficient for GaAs/AlGaAs parabolic quantum dots, and compare the results obtained considering excitonic effects with the ones obtained without considering them. The results show that the third-harmonic-generation coefficient is greatly enhanced when the exciton states in the quantum dots are considered—it is over three times bigger than that obtained when only considering electron states—and that it is very sensitively dependent on the exciton confinement. In addition, the third-harmonic-generation coefficient is related to the relaxation constant. Brief conclusions are given in section 5.

2. Excitons in parabolic quantum dots

The effective-mass Hamiltonian for an electron–hole pair in a parabolic quantum dot can be written as

$$H = \frac{\boldsymbol{p}_e^2}{2m_e^*} + \frac{1}{2}m_e^*\omega_0^2\boldsymbol{r}_e^2 + \frac{\boldsymbol{p}_h^2}{2m_h^*} + \frac{1}{2}m_h^*\omega_0^2\boldsymbol{r}_h^2 - \frac{e^2}{\epsilon|\boldsymbol{r}_e - \boldsymbol{r}_h|} \tag{1}$$

where m_e^* and m_h^* are the effective mass of the electron and hole, respectively. ω_0 is the frequency of the parabolic confining potential. The Coulomb interaction is screened by the background dielectric constant ϵ. Since all of the first four terms in equation (1) are quadratic and the Coulomb term depends only on the relative coordinate $\boldsymbol{r} = \boldsymbol{r}_e - \boldsymbol{r}_h$, it is easy to see that the Hamiltonian is separable into terms in the relative coordinate $\boldsymbol{r}$ and centre-of-mass coordinate $\boldsymbol{R}$, defined by

$$\boldsymbol{r} = \boldsymbol{r}_e - \boldsymbol{r}_h \qquad \boldsymbol{R} = \frac{m_e^*\boldsymbol{r}_e + m_h^*\boldsymbol{r}_h}{M}. \tag{2}$$

We also define the total mass

$$M = m_e^* + m_h^*$$

and the reduced mass

$$\mu = m_e^* m_h^*/M.$$

The electron and hole momenta $\boldsymbol{p}_e$ and $\boldsymbol{p}_h$ can be expressed in terms of the centre-of-mass momentum, $\boldsymbol{P} = (\hbar/\mathrm{i})\boldsymbol{\nabla}_{\boldsymbol{R}}$, and the relative momentum, $\boldsymbol{p} = (\hbar/\mathrm{i})\boldsymbol{\nabla}_{\boldsymbol{r}}$, as

$$\boldsymbol{p}_h = -\boldsymbol{p} + \boldsymbol{P}\frac{m_h}{M} \qquad \boldsymbol{p}_e = \boldsymbol{p} + \boldsymbol{P}\frac{m_e}{M}. \tag{3}$$

Substituting (2) and (3) in the Hamiltonian (1) yields

$$H = \frac{\boldsymbol{P}^2}{2M} + \frac{1}{2}M\omega_0^2\boldsymbol{R}^2 + \frac{\boldsymbol{p}^2}{2\mu} + \frac{1}{2}\mu\omega_0^2\boldsymbol{r}^2 - \frac{e^2}{\epsilon|\boldsymbol{r}|}. \tag{4}$$

The explicit separability of the $\boldsymbol{r}$- and $\boldsymbol{R}$-coordinates in (4) means that the exciton wave function, $\psi(\boldsymbol{r}_e, \boldsymbol{r}_h)$, satisfying the Schrödinger equation

$$H\psi(\boldsymbol{r}_e, \boldsymbol{r}_h) = E\psi(\boldsymbol{r}_e, \boldsymbol{r}_h) \tag{5}$$

can be written as

$$\psi(\boldsymbol{r}_e, \boldsymbol{r}_h) = \chi(\boldsymbol{R})\varphi(\boldsymbol{r}). \tag{6}$$

Obviously, $\chi(\boldsymbol{R})$ is the wave function of a two-dimensional (2D) harmonic oscillator, which has been solved as

$$E_{\boldsymbol{R}} = (2n + |m| + 1)\hbar\omega_0 \tag{7}$$

$$\chi(\boldsymbol{R}) = \frac{1}{\sqrt{2\pi}}\mathrm{e}^{\mathrm{i}m\theta}\left[\frac{2M\omega_0 n!}{\hbar(|m|+n)!}\right]^{1/2}\rho^{|m|}L_n^{|m|}(\rho^2)\mathrm{e}^{-(1/2)\rho^2} \tag{8}$$

where $m = 0, \pm1, \pm2, \ldots, n = 0, 1, 2, \ldots, \rho = R\sqrt{M\omega_0/\hbar}$, and $L_n^{|m|}$ are associated Laguerre polynomials.

The exciton energy can be written as the sum of the centre-of-mass part and the relative motion part, namely as $E = E_{\boldsymbol{R}} + E_r$. The problem now is reduced to solving the relative-motion Hamiltonian

$$H_r = \frac{\boldsymbol{p}^2}{2\mu} + \frac{1}{2}\mu\omega_0^2\boldsymbol{r}^2 - \frac{e^2}{\epsilon|\boldsymbol{r}|}. \tag{9}$$

The Hamiltonian (9) contains two length scales. One is the size of the quantum dot, defined by

$$R_0 = \sqrt{\hbar/\mu\omega_0}. \tag{10}$$

The other length scale is the exciton effective Bohr radius

$$a_B^* = \frac{\epsilon\hbar^2}{\mu e^2}. \tag{11}$$

There are also two energy scales. One is the energy quantum due to confinement, $\hbar\omega_0$, which is related to R_0 by

$$\hbar\omega_0 = \frac{\hbar^2}{\mu R_0^2}. \tag{12}$$

The other energy scale is the effective Rydberg [7]:

$$\Re^* = \frac{e^2}{\epsilon a_B^*} = \frac{\mu e^4}{\epsilon^2\hbar^2}. \tag{13}$$

The competition between the two length scales, or equivalently the competition between the two energy scales, defines the strong-confinement regime, where $R_0 \ll a_B^*$, or $\hbar\omega_0 \gg \Re^*$, and the weak-confinement regime, where $R_0 \gg a_B^*$, or $\hbar\omega_0 \ll \Re^*$. In the following, we will discuss the two cases individually.

In the strong-confinement regime where the Coulomb term is neglected, we have a harmonic oscillator. The eigenenergies and eigenstates of a 2D harmonic oscillator in terms of polar coordinates, angular momentum quantum number m, and radial quantum number n are given by

$$E_{nm} = (2n + |m| + 1)\hbar\omega_0 \tag{14}$$

$$\varphi(r) = \frac{1}{\sqrt{2\pi}} e^{im\theta} \left[\frac{2\mu\omega_0 n!}{\hbar(|m|+n)!} \right]^{1/2} \rho^{|m|} L_n^{|m|}(\rho^2) e^{-(1/2)\rho^2} \tag{15}$$

where $m = 0, \pm 1, \pm 2, \ldots$, $n = 0, 1, 2, \ldots$, $\rho = r\sqrt{\mu\omega_0/\hbar}$, and $L_n^{|m|}$ are associated Laguerre polynomials.

In the weak-confinement regime where the parabolic confinement term is neglected, we have a hydrogenic problem; therefore the Hamiltonian (9) can be simplified as $H_r = \boldsymbol{p}^2/2\mu - e^2/\epsilon r$. The Schrödinger equation for the 2D hydrogenic Hamiltonian is now exactly solvable, giving energy eigenvalues and eigenfunctions [7] as follows:

$$E_r = -\frac{\Re^*}{2(n + |m| + \frac{1}{2})^2} \tag{16}$$

$$\varphi(r) = \frac{1}{\sqrt{2\pi}} e^{im\theta} C_{nm} R_{nm}(r) \tag{17}$$

$$R_{nm}(r) = \rho^{|m|} L_n^{|2m|}(\rho) e^{-\rho/2} \tag{18}$$

$$\rho = \frac{2r}{a_B^*(n + |m| + \frac{1}{2})} \tag{19}$$

$$C_{nm} = \frac{4}{a_B^*} \left[\frac{n!}{(n+2|m|)!(2n+2|m|+1)^3} \right]^{1/2} \tag{20}$$

where $m = 0, \pm 1, \pm 2, \ldots$, $n = 0, 1, 2, \ldots$.

3. Third-harmonic generation in parabolic quantum dots

Next we will discuss the expression for the third-harmonic-generation coefficient in this model. Let us consider an electromagnetic field with frequency ω which is incident with a polarization vector normal to the quantum dot. The system is excited by an electromagnetic field

$$E(t) = E_0 \cos\omega t = \widetilde{E} e^{i\omega t} + \widetilde{E} e^{-i\omega t}. \tag{21}$$

Let ρ denote the one-electron density matrix for this regime. Then the evolution of the density matrix ρ obeys the following time-dependent equation:

$$\partial\rho_{ij}/\partial t = (i\hbar)^{-1} [H_0 - qrE(t), \rho]_{ij} - \Gamma_{ij}(\rho - \rho^{(0)})_{ij} \tag{22}$$

where H_0 is the Hamiltonian for this system without the electromagnetic field $E(t)$; q is the electronic charge; $\rho^{(0)}$ is the unperturbed density matrix; Γ_{ij} is the relaxation rate. Equation (22) is solved using the usual iterative method [11, 12]:

$$\rho(t) = \sum_n \rho^{(n)}(t) \tag{23}$$

with

$$\partial\rho_{ij}^{(n+1)}/\partial t = (i\hbar)^{-1} \left\{ \left[H_0, \rho^{(n+1)} \right]_{ij} - i\hbar\Gamma_{ij}\rho_{ij}^{(n+1)} \right\} - (i\hbar)^{-1} \left[qr, \rho^{(n)} \right]_{ij} E(t). \tag{24}$$

The electronic polarization of the quantum dots will also be a series expansion like equation (23). We shall limit ourselves to considering the first three orders, i.e.,

$$P(t) = (\varepsilon_0 \chi^{(1)} E_0 e^{i\omega t} + \varepsilon_0 \chi_{2\omega}^{(2)} E_0^2 e^{2i\omega t} + \varepsilon_0 \chi_{3\omega}^{(3)} E_0^3 e^{3i\omega t}) + \text{c.c.} \tag{25}$$

where $\chi^{(1)}$, $\chi^{(2)}_{2\omega}$, and $\chi^{(3)}_{3\omega}$ are the linear, second-harmonic-generation, and third-harmonic-generation coefficients, respectively. ε_0 is the vacuum permittivity. The electronic polarization of nth order is given by

$$P^{(n)}(t) = \frac{1}{S}\,\mathrm{Tr}(\rho^{(n)} qr) \tag{26}$$

where S is the area of interaction.

In this paper we shall focus on the third-harmonic generation; we can treat $H' = qrE(t)$ as a perturbation term. By using the same compact-density-matrix approach and iterative procedure as references [11, 12], we find that the third-harmonic-generation coefficient is given by

$$\begin{aligned}\chi^{(3)}_{3\omega} = \frac{q^4}{\varepsilon_0\hbar^3}\sum_i\sum_k \frac{\mu_{ki}}{3\omega-\omega_{ki}-\mathrm{i}\Gamma_{ki}}\sum_l\sum_j\Bigg[&\frac{\mu_{il}\mu_{lj}\mu_{jk}(\rho_k-\rho_j)}{(2\omega-\omega_{kl}-\mathrm{i}\Gamma_{kl})(\omega-\omega_{kj}-\mathrm{i}\Gamma_{kj})}\\ &-\frac{\mu_{il}\mu_{lj}\mu_{jk}(\rho_j-\rho_l)}{(2\omega-\omega_{kl}-\mathrm{i}\Gamma_{kl})(\omega-\omega_{jl}-\mathrm{i}\Gamma_{jl})}-\frac{\mu_{ij}\mu_{jl}\mu_{lk}(\rho_l-\rho_j)}{(2\omega-\omega_{li}-\mathrm{i}\Gamma_{li})(\omega-\omega_{lj}-\mathrm{i}\Gamma_{lj})}\\ &+\frac{\mu_{ij}\mu_{jl}\mu_{lk}(\rho_j-\rho_i)}{(2\omega-\omega_{li}-\mathrm{i}\Gamma_{li})(\omega-\omega_{ji}-\mathrm{i}\Gamma_{ji})}\Bigg]\end{aligned} \tag{27}$$

where $i, k, l, j = 0, 1, 2, 3$.

If the condition of two-photon resonance can be met, equation (27) can be simplified as

$$\begin{aligned}\chi^{(3)}_{3\omega} = \frac{q^4\mu_{01}\mu_{12}\mu_{23}\mu_{30}\rho_s}{\varepsilon_0\hbar^3}\Bigg[&\frac{1}{(3\omega-\omega_{21}-\mathrm{i}\Gamma_{21})(2\omega-\omega_{20}-\mathrm{i}\Gamma_{20})(\omega-\omega_{23}-\mathrm{i}\Gamma_{23})}\\ &+\frac{1}{(3\omega-\omega_{21}-\mathrm{i}\Gamma_{21})(2\omega-\omega_{20}-\mathrm{i}\Gamma_{20})(\omega-\omega_{30}-\mathrm{i}\Gamma_{30})}\\ &+\frac{1}{(3\omega-\omega_{23}-\mathrm{i}\Gamma_{23})(2\omega-\omega_{20}-\mathrm{i}\Gamma_{20})(\omega-\omega_{10}-\mathrm{i}\Gamma_{10})}\\ &+\frac{1}{(3\omega-\omega_{30}-\mathrm{i}\Gamma_{30})(2\omega-\omega_{20}-\mathrm{i}\Gamma_{20})(\omega-\omega_{21}-\mathrm{i}\Gamma_{21})}\\ &+\frac{1}{(3\omega-\omega_{30}-\mathrm{i}\Gamma_{30})(2\omega-\omega_{31}-\mathrm{i}\Gamma_{31})(\omega-\omega_{21}-\mathrm{i}\Gamma_{21})}\\ &+\frac{1}{(3\omega-\omega_{01}-\mathrm{i}\Gamma_{01})(2\omega-\omega_{31}-\mathrm{i}\Gamma_{31})(\omega-\omega_{32}-\mathrm{i}\Gamma_{32})}\\ &+\frac{1}{(3\omega-\omega_{21}-\mathrm{i}\Gamma_{21})(2\omega-\omega_{31}-\mathrm{i}\Gamma_{31})(\omega-\omega_{30}-\mathrm{i}\Gamma_{30})}\\ &+\frac{1}{(3\omega-\omega_{21}-\mathrm{i}\Gamma_{21})(2\omega-\omega_{31}-\mathrm{i}\Gamma_{31})(\omega-\omega_{01}-\mathrm{i}\Gamma_{01})}\Bigg]\end{aligned} \tag{28}$$

where ρ_s is the density of excitons in the quantum dots, ε_0 is the vacuum permittivity, $\omega_{ij} = (E_i - E_j)/\hbar$ is the Bohr frequency, $\mu_{ij} = |\langle\psi_j|r|\psi_i\rangle|$ is the off-diagonal matrix element ($i, j = 0, 1, 2, 3$).

4. Results and discussion

In the following, we will discuss the third-harmonic-generation coefficient $\chi^{(3)}_{3\omega}$ for GaAs/AlGaAs parabolic quantum dots in the weak-confinement and strong-confinement regimes. The parameters used in our numerical work are adopted as [13]: $m_e^* = 0.067m_0$, $m_h^* = 0.09m_0$ (m_0 is the mass of a free electron), $\rho_s = 5\times10^{24}$ m^{-3}, $\hbar\Gamma_{10} = \hbar\Gamma_{21} = \hbar\Gamma_{32} = \hbar\Gamma$ meV, $\hbar\Gamma_{20} = \hbar\Gamma_{31} = \hbar\Gamma/2$ meV, $\hbar\Gamma_{30} = \hbar\Gamma/3$ meV, $\epsilon = 13.1$.

4.1. Weak-confinement regime

In the weak-confinement regime, the frequency ω_0 of the parabolic confining potential should meet the criterion $\omega_0 \ll 1.0 \times 10^{13}\ \mathrm{s}^{-1}$.

Figure 1 shows the third-harmonic-generation coefficient $\chi^{(3)}_{3\omega}$ as a function of the photon energy $h\nu$ for four different values of relaxation constant $\hbar\Gamma$ with $\omega_0 = 1.0 \times 10^{12}\ \mathrm{s}^{-1}$: (a) $\hbar\Gamma = 0.45$ meV, (b) $\hbar\Gamma = 0.65$ meV, (c) $\hbar\Gamma = 1.5$ meV, (d) $\hbar\Gamma = 3.5$ meV, which are illustrated by the solid line, dotted line, dash–dotted line, and dashed line, respectively. It is obvious that there is a maximum peak value at $h\nu = 5.3$ meV, which originates from the three-photon resonance enhancement. We also observe another peak which starts at $h\nu = 7.2$ meV; this peak is mainly due to the two-photon resonance enhancement. A very important feature is that the smaller the relaxation constant $\hbar\Gamma$ is, the sharper the peak will be and the bigger the peak intensity will be. Also, when the relaxation constant $\hbar\Gamma = 3.5$ meV, the two-photon resonance will disappear, and the three-photon resonance will become not very obvious.

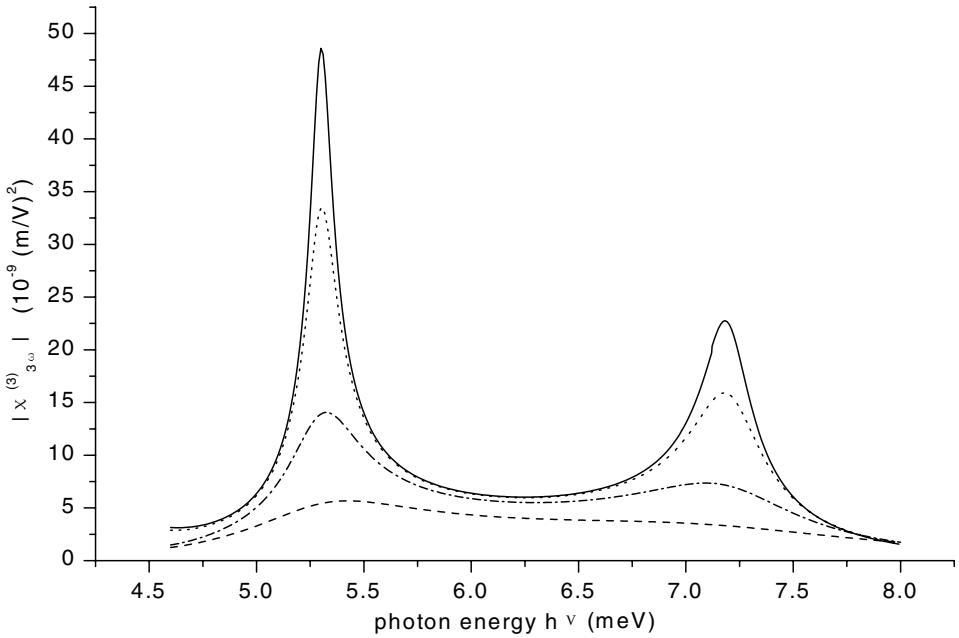

Figure 1. The third-harmonic-generation coefficient $|\chi^{(3)}_{3\omega}|$ versus the photon energy $h\nu$ for four different values of the relaxation constant $\hbar\Gamma$: (a) $\hbar\Gamma = 0.45$ meV, (b) $\hbar\Gamma = 0.65$ meV, (c) $\hbar\Gamma = 1.5$ meV, (d) $\hbar\Gamma = 3.5$ meV, which are illustrated by the solid line, dotted line, dash–dotted line, and dashed line, respectively.

Figure 2 shows the third-harmonic-generation coefficient $\chi^{(3)}_{3\omega}$ as a function of the frequency ω_0 of the parabolic confining potential with the relaxation constant $\hbar\Gamma = 0.45$ meV at the two-photon resonance. From figure 2, we can see that $\chi^{(3)}_{3\omega}$ will increase when the frequency ω_0 increases.

4.2. Strong-confinement regime

In the strong-confinement regime, the frequency ω_0 of the parabolic confining potential should meet the criterion $\omega_0 \gg 1.0 \times 10^{13}\ \mathrm{s}^{-1}$. In the following, we mainly discuss the two-photon resonance enhancement.

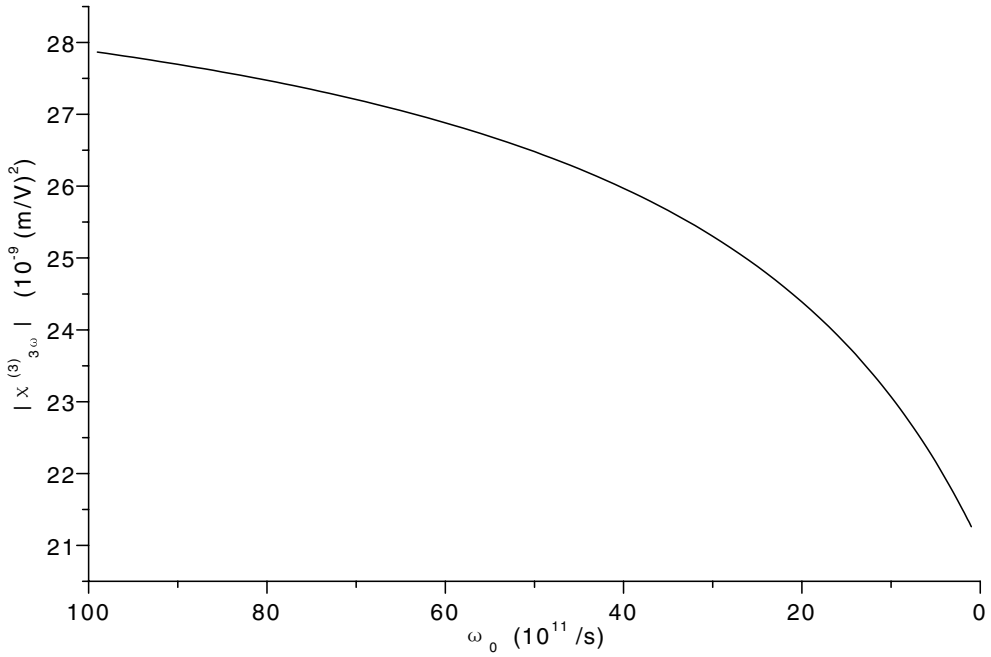

Figure 2. The third-harmonic-generation coefficient $|\chi^{(3)}_{3\omega}|$ versus the frequency ω_0 of the parabolic confining potential with the relaxation constant $\hbar\Gamma = 0.45$ meV at the two-photon resonance.

Figure 3 shows the third-harmonic-generation coefficient $\chi^{(3)}_{3\omega}$ as a function of the photon energy $h\nu$ for three different values of the parabolic confinement frequency ω_0: (a) $\omega_0 = 1.0 \times 10^{14}$ s^{-1}, (b) $\omega_0 = 2.0 \times 10^{14}$ s^{-1}, (c) $\omega_0 = 3.0 \times 10^{14}$ s^{-1}. We observe three peaks which start at $h\nu = 0.132$ eV, $h\nu = 0.263$ eV, $h\nu = 0.395$ eV, respectively. A very important feature is that the weaker the parabolic confinement is, the sharper the peak will be and the bigger the peak intensity will be. As the parabolic confinement frequency ω_0 increases, the peak will move to the right of the curve, which predicts a strong-confinement-induced blue-shift of the exciton resonance in semiconductor quantum dots in accordance with the recent experimental results [14]. These features make the parabolic quantum dots very promising candidates for nonlinear optical materials applications.

In figure 4, the third-harmonic-generation coefficient $\chi^{(3)}_{3\omega}$ is plotted as a function of the photon energy $h\nu$ with the relaxation constant $\hbar\Gamma = 0.45$ meV and $\omega_0 = 1.0 \times 10^{14}$ s^{-1}, for two cases: considering excitonic effects and not considering excitonic effects. From figure 4 we can see that the third-harmonic-generation coefficient $\chi^{(3)}_{3\omega}$ obtained considering excitonic effects is over three times larger than that obtained without considering excitonic effects—only considering electron states. The reason is that carriers in the semiconductor quantum dots are confined in three spatial dimensions, which substantially enhances the overlap between holes and electron clouds, and leads to enhancement of the Coulomb binding energy. Therefore it is apparently very important to take the excitonic effects into account when we study the third-harmonic-generation coefficient for quantum dots.

Figure 5 shows the third-harmonic-generation coefficient $\chi^{(3)}_{3\omega}$ as a function of the frequency ω_0 with the relaxation constant $\hbar\Gamma = 0.45$ meV, also for two cases: considering excitonic effects and not considering excitonic effects, which are illustrated by the solid line and dashed line, respectively. From figure 5 we can see that $\chi^{(3)}_{3\omega}$ will increase when the

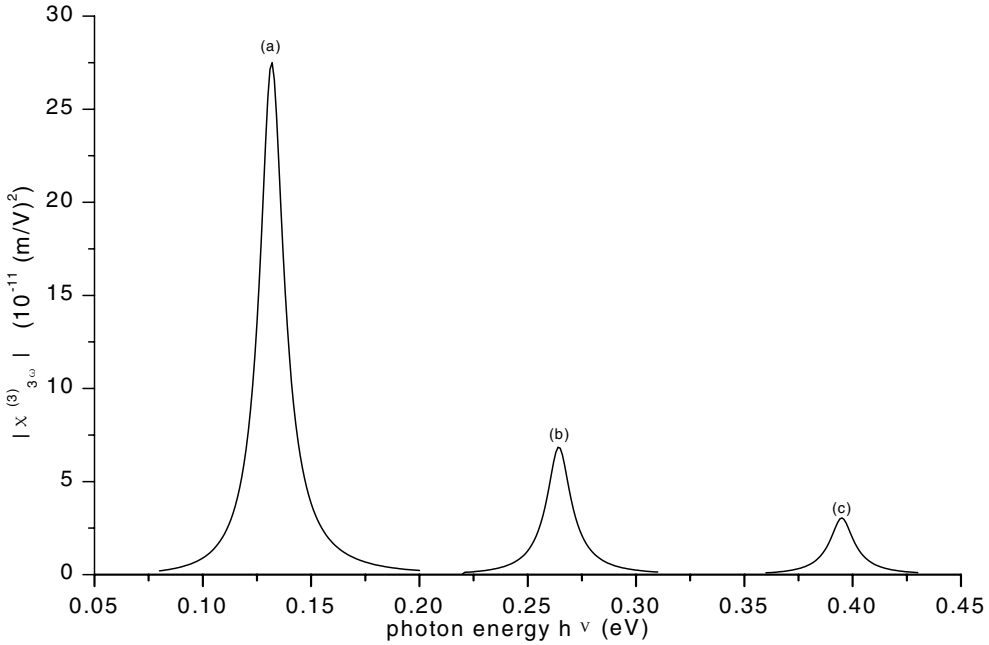

Figure 3. The third-harmonic-generation coefficient $|\chi^{(3)}_{3\omega}|$ versus the photon energy $h\nu$ for three different values of the parabolic confinement frequency ω_0: (a) $\omega_0 = 1.0 \times 10^{14}$ s^{-1}, (b) $\omega_0 = 2.0 \times 10^{14}$ s^{-1}, (c) $\omega_0 = 3.0 \times 10^{14}$ s^{-1}.

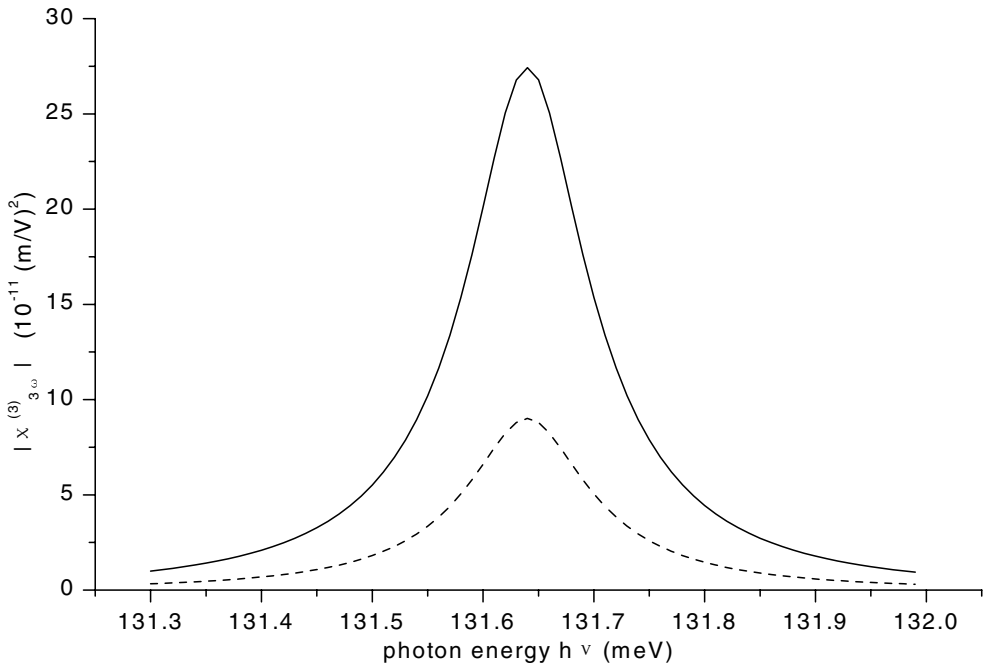

Figure 4. Frequency dispersion of the third-harmonic-generation coefficient $|\chi^{(3)}_{3\omega}|$ with the relaxation constant $\hbar\Gamma = 0.45$ meV, considering excitonic effects (solid line) and without considering excitonic effects (dashed line).

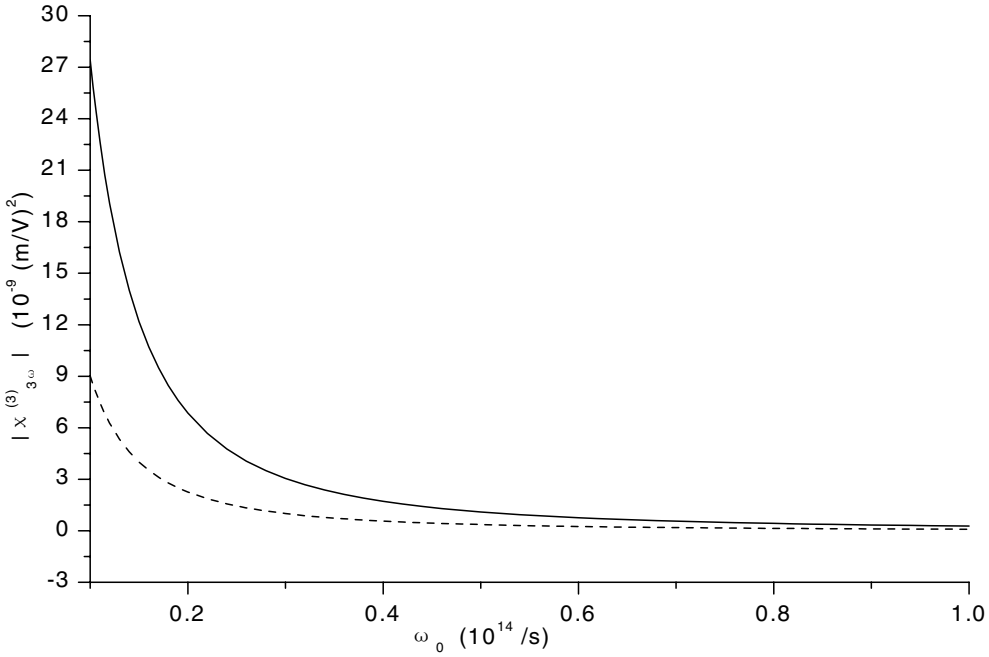

Figure 5. The third-harmonic-generation coefficient $|\chi^{(3)}_{3\omega}|$ versus the frequency ω_0 of the parabolic confining potential with the relaxation constant $\hbar\Gamma = 0.45$ meV, considering excitonic effects (solid line) and not considering excitonic effects (dashed line).

frequency ω_0 decreases, which is just the opposite to what happens in the weak-confinement regime. For the case where we consider excitonic effects, $\chi^{(3)}_{3\omega}$ will increase more quickly as ω_0 decreases than in the case where we do not consider excitonic effects; also, the third-harmonic-generation coefficient $\chi^{(3)}_{3\omega}$ obtained when considering excitonic effects is over three times larger than that obtained when excitonic effects are not considered. From figure 2 and figure 5, we can also see that the third-harmonic-generation coefficients $\chi^{(3)}_{3\omega}$ are essentially identical at the transition frequency $\omega_0 = 1.0 \times 10^{13}$ s^{-1}.

5. Conclusions

We present a simple and straightforward study of the third-harmonic-generation coefficient for a nanometre-size parabolic quantum dot. The results show that the theoretical value of the third-harmonic-generation coefficient $\chi^{(3)}_{3\omega}$ is greatly enhanced due to the excitonic effects and that $\chi^{(3)}_{3\omega}$ is very sensitively dependent on the exciton confinement. In the weak-confinement regime, $\chi^{(3)}_{3\omega}$ is over two orders of magnitude higher than that in the strong-confinement regime. Also, the smaller the relaxation constant $\hbar\Gamma$ is, the sharper the peaks will be and the bigger the peak intensities will be. However, the relaxation constant $\hbar\Gamma$ is related not only to the quantum dot material and confining potential, but also to other factors, such as temperature, boundary conditions, and electron–electron and exciton–exciton interactions. Therefore, theoretical study may make a great contribution to experimental studies, may have profound consequences as regards improvements of practical devices such as ultrafast optical switches, and may open up new opportunities for practical exploitation of the quantum-size effect in devices.

Acknowledgment

This work was supported by Natural Science Foundation of Guangdong Province.

References

[1] Ekimov A I, Efros Al L and Onushchenko A A 1985 *Solid State Commun.* **56** 921
[2] Brus L E 1986 *IEEE J. Quantum Electron.* **22** 1909
[3] Kash K *et al* 1986 *Appl. Phys. Lett.* **49** 1043
[4] Miyamoto Y *et al* 1987 *Japan. J. Appl. Phys.* **26** 225
[5] Guo Kangxian and Chen Chuanyu 1997 *J. Infrared Millimetre Waves* **16** 93
[6] Reed M A *et al* 1988 *Phys. Rev. Lett.* **60** 535
[7] Que Weiming 1992 *Phys. Rev.* B **45** 11 036
[8] Sauvage S and Boucaud P 1999 *Phys. Rev.* B **59** 9830
[9] Takagahara T 1989 *Phys. Rev.* B **39** 10 206
[10] Chen R, Lin D L and Mendoza B 1993 *Phys. Rev.* B **48** 11 879
[11] Rosencher E and Bois Ph 1991 *Phys. Rev.* B **44** 11 315
[12] Ahn Doyeol and Chuang Shun-lien 1987 *IEEE J. Quantum Electron.* **23** 2196
[13] Guo Kangxian and Chen Chuanyu 1998 *Acta Photon. Sinica* **27** 494
[14] Banyai L and Koch S W 1986 *Phys. Rev. Lett.* **57** 2722